
UNCONDITIONAL LATENT DIFFUSION MODELS MEMORIZE PATIENT IMAGING DATA

A PREPRINT

Salman Ul Hassan Dar^{1,2,3}

Marvin Seyfarth¹

Jannik Kahmann⁴

Isabelle Ayx⁴

Theano Papavassiliu^{2,3,5}

Stefan O. Schoenberg^{2,4}

Sandy Engelhardt^{1,2,3}

¹Department of Internal Medicine III, Heidelberg University Hospital, Germany

²AI Health Innovation Cluster (AIH), Germany

³German Centre for Cardiovascular Research (DZHK), Partner site Heidelberg/Mannheim, Germany

⁴Department of Radiology and Nuclear Medicine, University Medical Center Mannheim, Germany

⁵First Department of Medicine-Cardiology, University Medical Centre Mannheim, Germany

February 5, 2024

ABSTRACT

Generative latent diffusion models hold a wide range of applications in the medical imaging domain. A noteworthy application is privacy-preserved open-data sharing by proposing synthetic data as surrogates of real patient data. Despite the promise, these models are susceptible to patient data memorization, where models generate patient data copies instead of novel synthetic samples. This undermines the whole purpose of preserving patient data and may even result in patient re-identification. Considering the importance of the problem, surprisingly it has received relatively little attention in the medical imaging community. To this end, we assess memorization in latent diffusion models for medical image synthesis. We train 2D and 3D latent diffusion models on CT, MR, and X-ray datasets for synthetic data generation. Afterwards, we examine the amount of training data memorized utilizing self-supervised models and further investigate various factors that can possibly lead to memorization by training models in different settings. We observe a surprisingly large amount of data memorization among all datasets, with up to 41.7%, 19.6%, and 32.6 % of the training data memorized in CT, MRI, and X-ray datasets respectively. Further analyses reveal that increasing training data size and using data augmentation reduce memorization, while over-training enhances it. Overall, our results suggest a call for memorization-informed evaluation of synthetic data prior to open-data sharing.

Keywords · Contrastive Learning · Latent Diffusion · Memorization · Patient Privacy

1 Introduction

Contemporary developments in deep diffusion probabilistic models (DDPMs) have led to a significant leap in performance level in various medical imaging applications such as image segmentation, [1] reconstruction [2], synthesis [3], anomaly detection [4] and numerous others [5]. A notable application is open-data sharing for advancing medical imaging research while preserving patient privacy [6]. In open-data sharing, generative models are first trained to learn data distribution from private medical imaging datasets. Afterwards, generative models are used to generate synthetic samples, and since these synthesized samples do not belong to any specific patient, they can be shared publicly without compromising patient privacy. As a matter of fact, very recently, several studies have trained generative models on private/limited-access/restricted datasets and made synthetic data [6] or trained generative models [7, 8] publicly available.

Despite the potential of generative models for open data sharing, an underlying assumption is that the generated samples are novel and not mere patient data replicas. This is crucial, as the primary motivation for using synthetic data as surrogates of real patient data is to preserve patient privacy and synthesizing patient data copies circumvents the goal. A synthesized copy can even be traced back to the original patient, leading to patient re-identification [9]. Given the sensitive nature of patient medical data, surprisingly there has been little focus on the potential of such models to memorize training data and synthesize patient data replicas. On the contrary, the emphasis is typically on improving validation error or metrics that quantify image quality such as Fréchet inception distance (FID) or diversity such as multi-scale structural similarity index measure (MS-SSIM), without taking into consideration the memorization capacities of such models. However, despite their widespread usage as quantitative metrics during model training, FID and SSIM have several inherent limitations [10], which makes it difficult to determine the appropriate number of training epochs. Likewise, the validation loss itself only provides auxiliary information regarding model training. Therefore, exploring memorization-informed metrics during model training can be beneficial [10].

It could be argued that memorization could be mitigated by simply tracking validation error and avoiding over-fitting. However, this assumes equivalency between over-fitting and memorization. While the two terms might sometimes be correlated, this categorization is inaccurate [11]. Over-fitting is a global phenomenon where models attain very high accuracy on the training data typically at the expense of test data accuracy. Memorization, on the other hand, corresponds to the assignment of very high likelihood values to training data points. As a matter of fact, memorization of a model can be enhanced even when validation loss decreases, especially in the earlier phases of training when memorization might be increasing but the test loss might be decreasing [11].

To date, only a handful of studies have investigated patient data memorization in medical imaging [12, 13, 14]. Akbar et al. [14] assessed memorization in 2D diffusion models, and observed higher pixel-wise correlation among synthetic and real training samples as opposed to real test and training samples. In our previous work [12], we conducted experiments on 3D imaging datasets and utilized contrastive learning for detecting patient data replicas among the synthesized samples in a lower dimensional latent space. In another recent work, we showed that overtraining can lead to enhanced memorization [13]. Taken together, these studies suggest patient data memorization in unconditional diffusion models, and warrant a more thorough investigation regarding underlying reasons, and how it could be mitigated. Here, we build on our previous works [12, 13] by performing a thorough investigation on memorization in unconditional diffusion models for medical imaging. We train models on medical images to learn data distributions and perform copy detection via self-supervised models trained based on contrastive learning. Demonstrations on multiple 2D and 3D imaging datasets suggest that state-of-the-art diffusion models suffer from patient data memorization. Furthermore, several factors including training data size, training epochs, and data augmentation can have an impact on model’s memorization.

As a means to understand memorization in unconditional diffusion models, we pose the following questions:

- Is patient data memorization prevalent among medical imaging datasets having different properties?
- How can we detect memorization?
- Is there a relation between memorization and traditional quantitative metrics such as FID, and MS-SSIM used for training and assessment of generative models?
- Can memorization be used as a metric to assess generative models during training?
- How does training data size affect memorization?
- Can data augmentation alleviate memorization?

2 Methods

2.1 Latent Diffusion Models

Latent diffusion models (LDMs) belong to a family of likelihood-based generative models that are designed to learn data distribution $p(x)$ through a gradual denoising process in a low dimensional latent space [15]. The latent space is learned through an autoencoder. Given an image x , the encoder E_{θ_E} projects x onto its low dimensional latent representation z , followed by a back projection onto the original pixel space as \hat{x} . This latent space project reduces computational complexity and enables application on high-resolution images [15]. The autoencoder is trained using a reconstruction loss (\mathcal{L}_{rec}) that enforces the model to learn a meaningful compressed representation, and adversarial (\mathcal{L}_{adv}) and perceptual (\mathcal{L}_{perc}) losses for enhanced perceptual quality of the reconstructed image. The cumulative loss (\mathcal{L}_{com}) can be expressed as:

$$\mathcal{L}_{com} = \lambda_{rec}\mathcal{L}_{rec} + \lambda_{adv}\mathcal{L}_{adv} + \lambda_{perc}\mathcal{L}_{perc} \quad (1)$$

where λ_{rec} , λ_{adv} , and λ_{perc} are the loss weightings.

After learning the latent space, deep diffusion models undergo training in the latent space. Deep diffusion models are

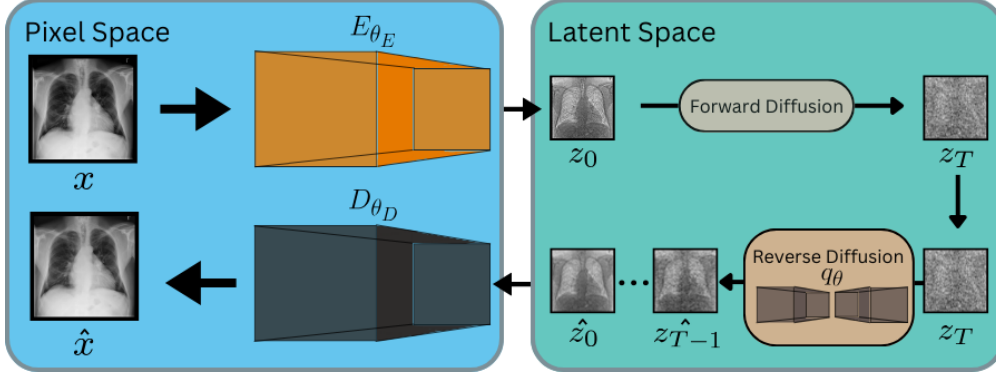


Figure 1: Latent Diffusion Models project data onto a lower dimensional latent space and perform gradual denoising followed by projection back onto the pixel space.

trained with the aim to minimize the upper variational bound of the negative log-likelihood of the data distribution $-\log(p(z))$ [16]. Training a diffusion model consists of two steps. The first step constitutes a forward diffusion process where normally distributed noise is added to the latent representation z of images x . This process is performed in small increments (δt) with a variance schedule of (β_t) , resulting in noisy representations z_t at every value of t . At any time t , $q(z_t|z_{t-1})$ is modelled as a normal distribution with mean $\sqrt{1 - \beta_t}z_{t-1}$ and variance β_t . The second step consists of a reverse diffusion process aimed at learning $q(z_{t-1}|z_t)$. Unlike $q(z_t|z_{t-1})$, $q(z_{t-1}|z_t)$ does not have a closed form expression and is typically estimated using a deep neural network $\hat{q}_{\theta}(z_{t-1}|z_t)$ at various different values of t .

Once the models are trained, they can be used to generate samples by initiating from random noise $z_T \sim \mathcal{N}(0, I)$ and performing sequential denoising to obtain a new sample z'_0 in the latent space. This new latent sample can be projected back to the pixel space using the decoder D_{θ_D} .

2.2 Memorization Assessment

Despite the ability of latent diffusion models to generate high-quality and realistic samples, the affinity of such models to memorize patient data and synthesize it has received little attention [12, 13, 14]. Nonetheless, before proceeding, it is important to define what constitutes memorization. Akbar et al. [14] defined memorization as a phenomenon where generative models synthesize patient data copies and copies as synthesized samples that are identical to training samples. Dar et al. [12] further expanded the definition of copies to further include variations such as rotation, flipping, and minor changes in contrast. Here we adhere to this definition, and drawing inspiration from Fernandez et al. [17] we formally define memorization as follows:

A training data sample x is considered to be (l, ρ) -memorized by a generative model G_{θ} if $l(x, v(\hat{x})) \geq \tau$, where \hat{x} is a sample extracted from G_{θ} using sampling algorithm A , v corresponds to minor variations such rotation, flipping and slight changes in contrast, and l is the similarity between the samples. Under such conditions, \hat{x} is defined as a copy of x .

2.2.1 Contrastive Learning

One naive way to detect patient data copies is to compare each synthesized sample with all training samples and select the samples showing a similarity level greater than the threshold τ as copies. However, this approach is computationally inefficient and is not suitable for detecting copies that are variations of patient images. Accordingly, we utilized self-supervised models that project images into a lower dimensional embedding space and used a contrastive learning approach to bring each training sample closer to its variation and push away from other samples. The rationale behind this approach is that copies would lie closer to the training samples and novel samples would be far away.

Consider a batch $B = [y_1, y_2, \dots, y_K]$ containing K samples, where y_i corresponds to i^{th} sample. After obtaining variation y'_i for each sample y_i , the modified batch can then be represented as $B' = [y_1, y'_1, y_2, y'_2, \dots, y_K, y'_K]$. One straightforward way is to form a positive (y_i, y'_i) and a negative pair (y_i, y_j) for each sample y_i . However, we observed that such an approach was unable to efficiently push samples within a negative pair away from each other. Therefore we increased the number of negative pairs for each sample, such that for each sample y_i negative pairs were formed using all other samples in the batch, making $2(K - 1)$ negative pairs per sample.

The self-supervised model SS_{θ} model was trained using the normalized temperature-scaled cross entropy (NT-Xent) loss [18]. First, SS_{θ} was used to obtain embeddings $E = [e_1, e'_1, e_2, e'_2, \dots, e_K, e'_K]$ of all samples within B' . For each

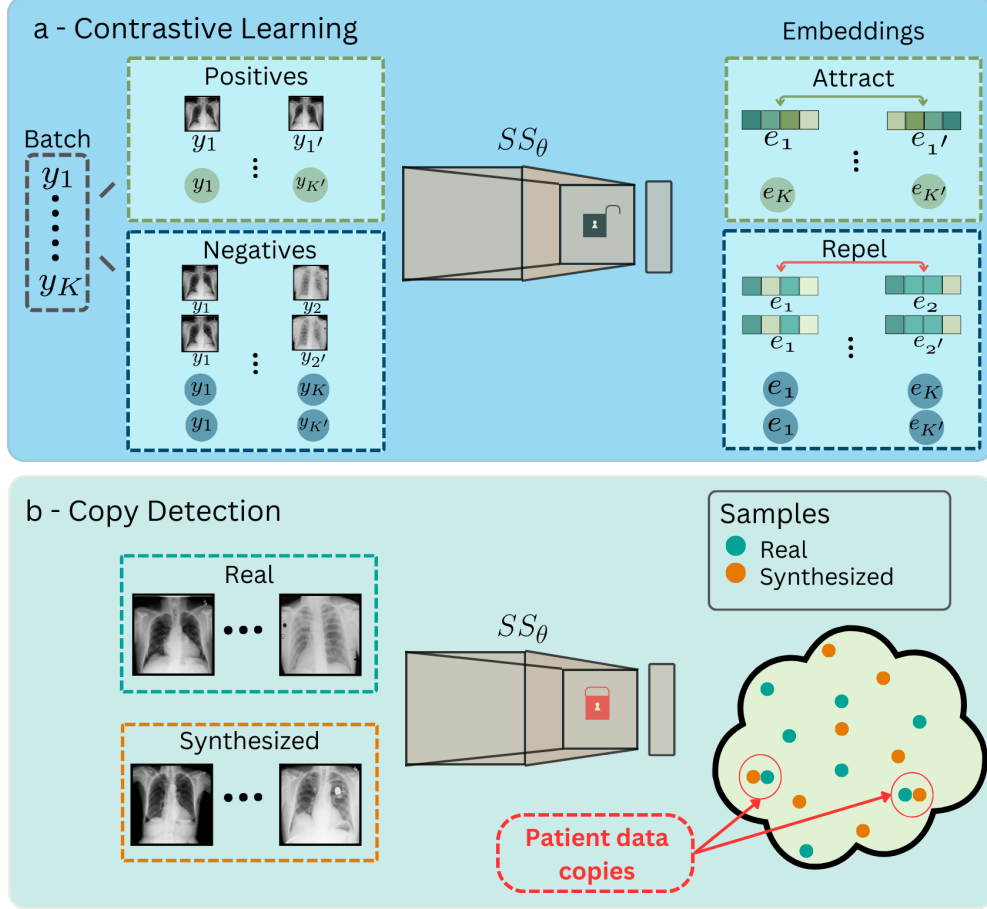


Figure 2: a - Self-supervised model is trained to project images onto a lower dimensional embedding space where each sample within a batch is brought closer to its variation and pushed far away from all other samples in the batch. b - Patient data copies are detected by projecting all training and synthetic samples onto the embedding space and identifying the training synthetic pairs lying close to each other.

i th sample it was then updated based on the NT-Xent loss function, expressed as follows:

$$\mathcal{L}_i = -\log \frac{e^{(s_{e_i, e_i'} / \tau)}}{\sum_{j=1}^{2K} \mathbb{1}_{[j \neq i]} e^{(s_{e_i, e_j} / \tau)}} + \frac{e^{(s_{e_j', e_j} / \tau)}}{\sum_{j=1}^{2K} \mathbb{1}_{[j \neq i']} e^{(s_{e_i', e_j} / \tau)}} \quad (2)$$

Here s_{e_i', e_j} is cosine similarity i th and j th embeddings and $\mathbb{1}_{[j \neq i]}$ is the indicator function which is 1 when $j \neq i$ and 0 when $j = i$.

2.2.2 Copy Detection

For the detection of patient data copies, SS_θ was first utilized to obtain embeddings of all training, validation, and synthetic samples. Next, Pearson's correlation coefficient was computed between all pairs of training-validation embeddings (ρ_{tr-val}), and training-synthetic embeddings (ρ_{tr-syn}). Afterwards, for each training embedding, the closest validation embedding was selected to form a distribution of their correlation values (ρ_{NN-val}). A threshold value (τ) was then defined as 95th percentile of ρ_{NN-val} . Finally, for each training embedding the closest synthetic embedding was selected (ρ_{NN-syn}), and training samples with ρ_{NN-syn} greater than τ were categorized as memorized. Algorithm 1 demonstrates the copy detection process via a pseudo code.

2.3 Datasets

The proposed approach was demonstrated on three medical imaging datasets. To evaluate the prevalence of memorization in medical images, we selected datasets covering a range of imaging modalities, anatomies, image

Algorithm 1: Copy detection

Input: $E_{tr} = [e_{tr}^1, \dots, e_{tr}^{N_{tr}}]^T \in \mathbb{R}^{N_{tr} \times L}$: N_{tr} training embeddings of length L
 $E_{val} = [e_{val}^1, \dots, e_{val}^{N_{val}}]^T \in \mathbb{R}^{N_{val} \times L}$: N_{val} validation embeddings
 $E_{syn} = [e_{syn}^1, \dots, e_{syn}^{N_{syn}}]^T \in \mathbb{R}^{N_{syn} \times L}$: N_{syn} synthetic embeddings
 $corr(., .)$: Pearson’s correlation between inputs
 $percentile(., u)$: u th percentile of input vector
 $ind()$: Indices of True values
Output: ID_{cop} : Indices of memorized samples

- 1 $\rho_{tr-val} = corr(E_{tr}, E_{val}) \in \mathbb{R}^{N_{tr} \times N_{val}}$ // Pairwise correlations between embeddings
- 2 $\rho_{tr-syn} = corr(E_{tr}, E_{syn}) \in \mathbb{R}^{N_{tr} \times N_{syn}}$
- 3 $\rho_{NN-val} = max(\rho_{tr-val}) \in \mathbb{R}^{N_{tr}}$ // Nearest neighbor selection for each training embedding
- 4 $\rho_{NN-syn} = max(\rho_{syn-val}) \in \mathbb{R}^{N_{tr}}$
- 5 $\tau = percentile(\rho_{NN-val}, 95)$ // Threshold based on 95 percentile
- 6 $ID_{cop} = ind(\rho_{NN-syn} \geq \tau)$ // Indices of training samples that are memorized

resolutions, field of views, and spatial dimensions. The details of the datasets are as follows:

Chest X-ray: A publicly available 2D chest X-ray dataset (X-ray) was considered [19]. A subset of 20,000 images was analyzed for reduced computational complexity, where 10,000 were reserved for training and 10,000 for validation.

Knee MRI: A publicly available 3D knee MRI dataset (MRNet) was analyzed [20], where MR volumes of 904 subjects were used for training and 226 for validation.

Photon counting Computer Tomography Angiography (PCCTA): 3D-PCCTA data of 65 coronary artery disease (CAD) patients were acquired at the Mannheim University Hospital. Plaques within coronary arteries were labeled and more focused volumes of sizes $64 \times 64 \times 64$ surrounding plaques were analysed, making 242 volumes for training and 58 for validation.

2.4 Networks and Training Details

For training LDMs on the 2D X-ray dataset training procedures, network architectures, and hyperparameters were adopted from an online repository (https://github.com/Warvito/generative_chestxray) built on MONAI framework [21]. For training LDMs on 3D datasets, training procedures, network architectures, and hyperparameters were adopted from [22].

For training 2D self-supervised models, the architecture was adopted from [9] with minor modifications, including changing the number of input layer channels to 1 and replacing the output classification layer with a fully connected layer mapped to a 128-dimensional vector. Training was performed for 200 epochs using Adam optimizer with cosine annealing learning rate schedule, where the learning rate was reduced from 10^{-4} to 5×10^{-3} . For training 3D self-supervised models, the encoder from the LDM architecture was utilized.

3 Results

3.1 Memorization in Generative Models

We first assess memorization in LDMs trained on all three datasets by detecting copies among the synthesized images. Theoretically, for a model that perfectly learns data distribution, there is always a non-zero probability of synthesizing patient data copies. Consequently, a synthetic dataset consisting of infinite samples should also contain all training samples. Therefore, the key question comprises determining a relatively higher likelihood assigned to the training images as opposed to novel images in the distribution not seen during training. To answer this question, we synthesized a finite number of samples N_{syn} by setting it equal to the training data size (N_{train}). LDMs trained on each dataset were used to synthesize novel images (Fig. 1). Afterwards, the self-supervised models were used to detect potential replicas of training samples among the synthesized samples (Fig. 2). Fig. 3 shows the distribution of correlation values between training and nearest validation embeddings (ρ_{NN-val}), and between training and nearest synthetic embeddings (ρ_{NN-syn}). In all datasets, ρ_{NN-syn} are shifted more towards the right compared to ρ_{NN-val} , implying that synthetic samples bear a higher resemblance to the training data. Next, we quantify the amount of training samples that the model memorized as mentioned in Section. 2.2.2. In (PCCTA, MRNet) datasets, (41.7, 19.6) % of the training data are memorized, and (76.9, 35.5) % of the synthetically generated samples are identified as patient data copies. Fig. 4

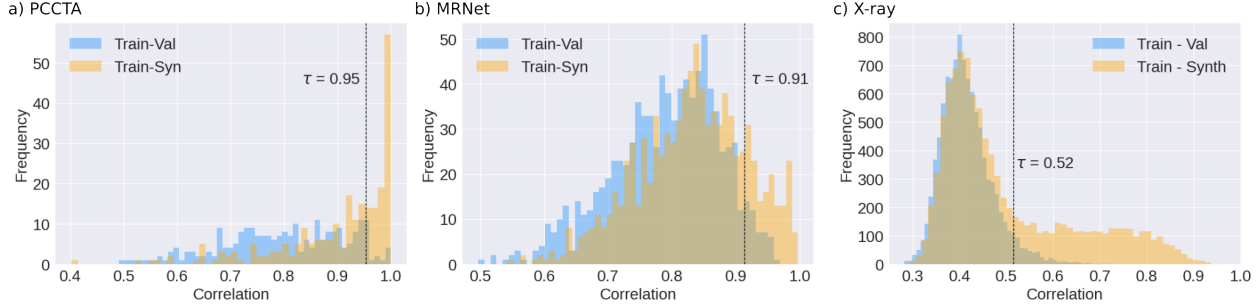


Figure 3: Histograms showing distributions of Pearson’s correlation values among closest training-validation pairs (blue) and training-synthetic pairs (orange) in a) PCCTA, b)MRNet, and c)X-Ray datasets.

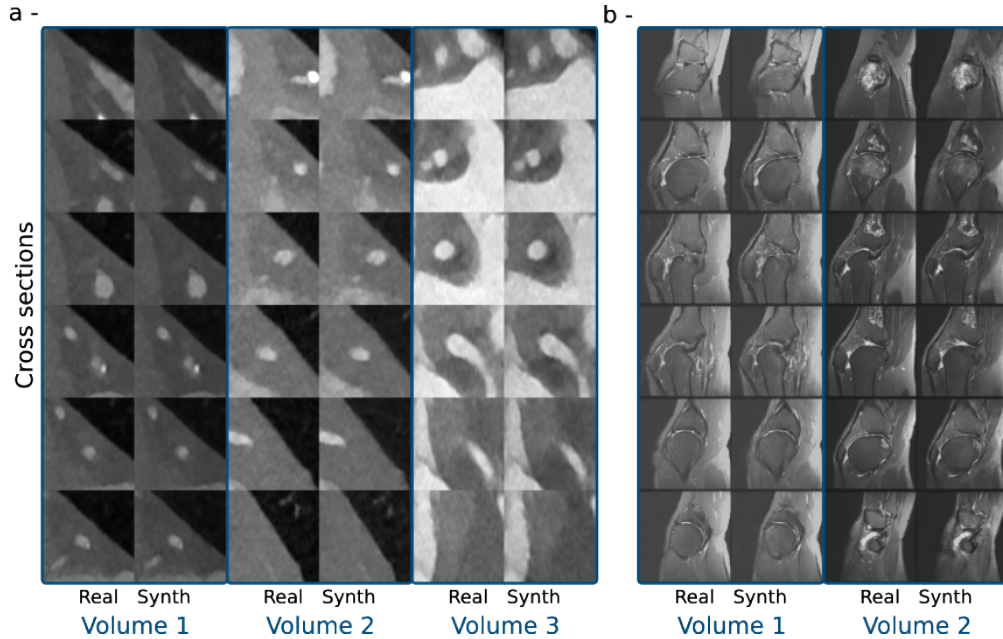


Figure 4: Representative cross sections of real and detected copies in a) PCCTA and b) MRNet datasets. Copies show a high resemblance to the corresponding real samples.

shows copies along with the closest training samples. In the PCCTA dataset, which contains low-dimensional images, most of the details are preserved in the memorized samples. In the MRNet dataset, which contains high-resolution and detailed images, most of the global structure is preserved, albeit with notable differences in fine structural details. These differences can be attributed to the inability of the model to capture low-level details in the 3D images. In the 2D X-ray dataset, 32.6 % of the training data are memorized and 54.5% of the synthetic samples are patient data copies. Fig. 5 shows copies alongside the closest training samples. Synthetic samples show a very close resemblance to the training samples. An intriguing observation is regarding the difference in memorization among all datasets. PCCTA has the highest memorization percentage, followed by X-ray and finally MRNet. However, a direct comparison is not possible due to differences in imaging modality, spatial resolution, field of view, anatomy, and structural details.

3.2 Copy Detection

Next, we gauge the effectiveness of the self-supervised models in detecting copies. The correlation threshold τ used to categorize samples as copy or novel is based on the 95th percentile of the correlation values between training and nearest validation sample embeddings. To evaluate if the selected threshold value τ is meaningful, we also randomly selected 100 training and nearest synthetic sample pairs, and manually labeled the corresponding synthesized samples as novel or copies. These labels were then compared with the ones obtained based on τ . In the PCCTA dataset, copies

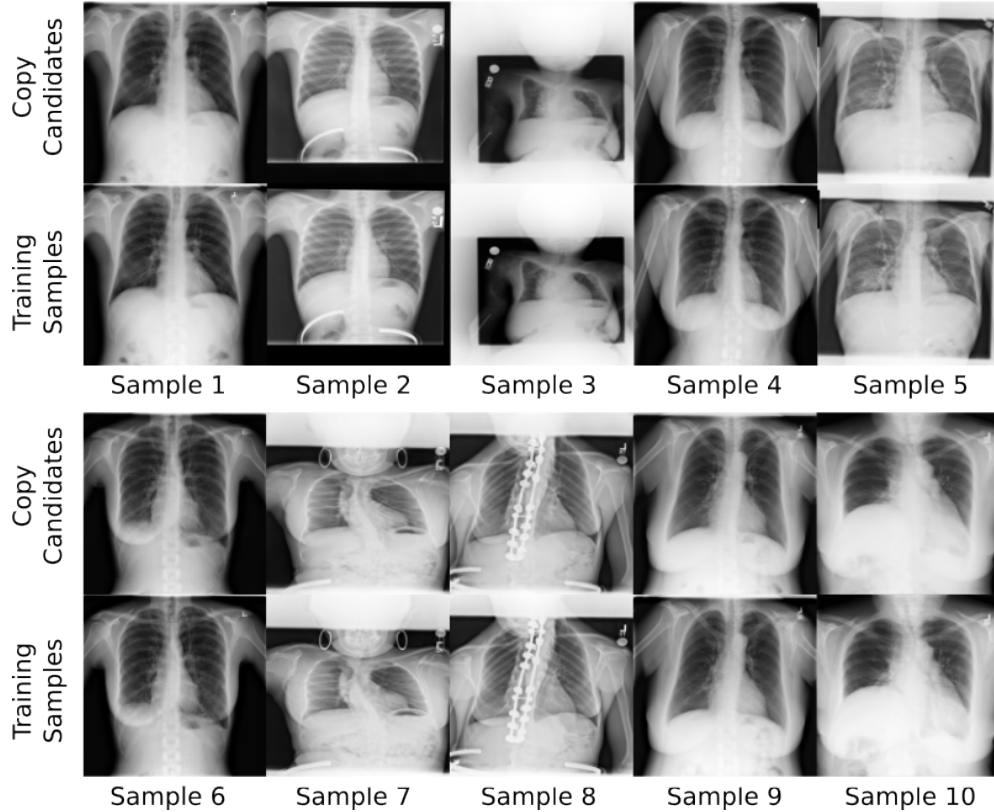


Figure 5: Representative cross sections of real and detected copies in X-ray dataset. Copy candidates show a high resemblance to the corresponding real samples. The network tends to copy even the exact position of the image in case of partial field of view coverage.

are detected with sensitivity of 81% and specificity of 75%. In the MRNet dataset, copies are detected with sensitivity of 60% and specificity of 92%. In the X-ray dataset, copies are detected with sensitivity of 85% and specificity of 94%.

3.3 Factors Affecting Memorization

Next, we investigated the factors that could potentially influence memorization. For this purpose, we opted for the X-ray dataset, the main reason being that it is a large dataset that provides us with the freedom to analyze multiple different aspects of memorization.

3.3.1 Training Data Size

Deep neural networks are prone to overfitting upon training on small datasets. Although overfitting and memorization are two distinct concepts, overfitting can lead to memorization. LDMs learn data generation through gradual denoising an inherently ill-posed problem with infinitely many solutions. Training LDMs on small datasets makes the models overfit to solutions leading to denoised training images. This can in turn increase the likelihood of generating more training samples at random. To explore this phenomenon, we investigated the effect of training data size (N_{train}) on memorization. We compared the LDMs trained for $N_{train} = (5k, 10k, 20k)$ images denoted as $(G_{\theta,5k}, G_{\theta,10k}, G_{\theta,20k})$ respectively. The self-supervised model was trained on 20k training images. Among the 5k shared training images among all models, (54.7, 31.8, 16.2)% of the training samples are memorized in $(G_{\theta,5k}, G_{\theta,10k}, G_{\theta,20k})$ and (68.6, 51.8, 39.8)% of the synthesized samples are identified as copies in $(G_{\theta,5k}, G_{\theta,10k}, G_{\theta,20k})$. Fig. 6a also shows distributions among correlation values of training samples and nearest synthetic samples along with the mean values. If we consider all images used for training of $(G_{\theta,5k}, G_{\theta,10k}, G_{\theta,20k})$ respectively, (54.7, 33.2, 17.7)% of the training samples are memorized in $(G_{\theta,5k}, G_{\theta,10k}, G_{\theta,20k})$ and (68.6, 51.4, 39.9)% of the synthesized samples are copies in $(G_{\theta,5k}, G_{\theta,10k}, G_{\theta,20k})$ Fig. 6b also shows distributions among correlation values of training samples and nearest synthetic samples

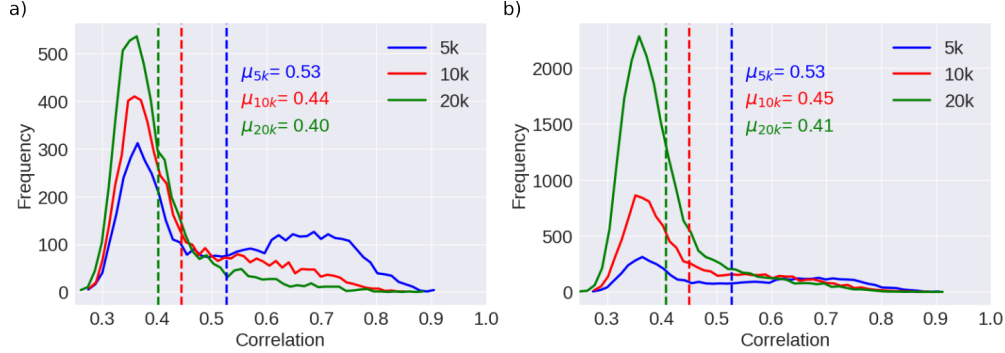


Figure 6: Distributions of Pearson’s correlation coefficient between training and nearest synthetic samples for $G_{\theta,5k}$, $G_{\theta,10k}$ and $G_{\theta,20k}$ with their respective mean values (μ_{5k} , μ_{10k} and μ_{20k}). a) 5k shared training samples are considered for all models. b) (5k, 10k, 20k) training samples are considered for ($G_{\theta,5k}$, $G_{\theta,10k}$, $G_{\theta,20k}$). Both histograms suggest a negative correlation between N_{train} and the similarity between training and nearest synthesized samples.

along with the corresponding mean values. The results suggest that increasing the training set size tends to decrease the percentage memorization.

3.3.2 Training Iterations

One aspect of LDMs that receives little attention is the number of iterations or epochs used for training, and most of the studies just report a number without performing a thorough evaluation. Overtraining the network can make the network overfit to the training data while denoising, and can lead to more frequent generation of training samples during progressive denoising. This can lead to enhanced memorization [13]. To assess the effect of training epochs/iterations

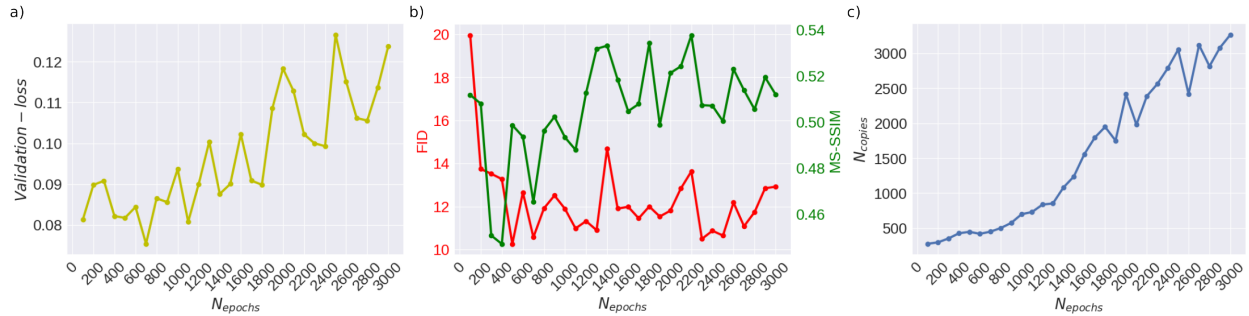


Figure 7: a) Validation loss between denoised samples and corresponding reference images during training of LDMs, b) FID between synthesized and real images, b) MS-SSIM within the synthesized data, and c) Number of copies (N_{copies}) as a function of number of epochs (N_{epochs}) used for training are shown.

on memorization of LDMs, we trained LDMs for epochs in the range [100,3000]. Fig. 7 shows the number of copies (N_{copies}) detected as a function of training epochs. N_{copies} increases with training epochs, suggesting that over-training the model can lead to enhanced memorization. In addition to the relation between N_{copies} and N_{epochs} , we were also interested in evaluating their relation with metrics conventionally used for assessment or training of generative models. For this purpose, we also calculated FID, MS-SSIM, and validation error as a function of N_{epochs} . Validation error initially decreases then starts increasing after around 700 epochs. However, it is worth noting that the validation error just gives an indication regarding the denoising abilities of the model and provides little information regarding the generative capabilities of the network. FID decreases till 500 epochs, and then oscillates afterwards. It implies that image quality saturates after a specific number of epochs. MS-SSIM shows a decreasing trend till 400 epochs, increases, and then starts oscillating. One thing to consider is that MS-SSIM only quantifies diversity and does not provide any information regarding image quality. Collectively, the curves suggest somewhere between 400-700 epochs seems to be the optimum point. However, generative models are generally trained for several days assuming that they would learn to generate high-quality samples. Not only can this enhance memorization, but it can also be sub-optimal in terms of typically used quantitative metrics. Taken together, our results suggest that memorization is an aspect that should be

taken into account while training generative models, and perhaps a hybrid metric could be used for training of models for open-data sharing [10].

3.3.3 Data augmentation

Data augmentation is a widely used technique that artificially expands the training dataset size by complementing it with variations of training samples. This typically enhances generalizability in deep neural networks, potentially reducing memorization in LDMs [12]. Here, we also assess memorization in LDMs by training models on expanded datasets obtained via augmentation techniques. In each epoch, all training samples underwent flipping and rotation ($-5^\circ, 5^\circ$) operations with a probability of 50% each. We observe that in augmented models 5.6% of the training samples are memorized, and 7.3% of the synthesized samples are copies. This is approximately 6 times less than the models trained without augmentation. A careful examination of the copies shows that although such models synthesize patient data copies, the patient data copies are not just augmented versions of the original patient image. These copies also contain some notable minor variations. Fig. 8 shows some of the selected copies. One potential explanation is that such models

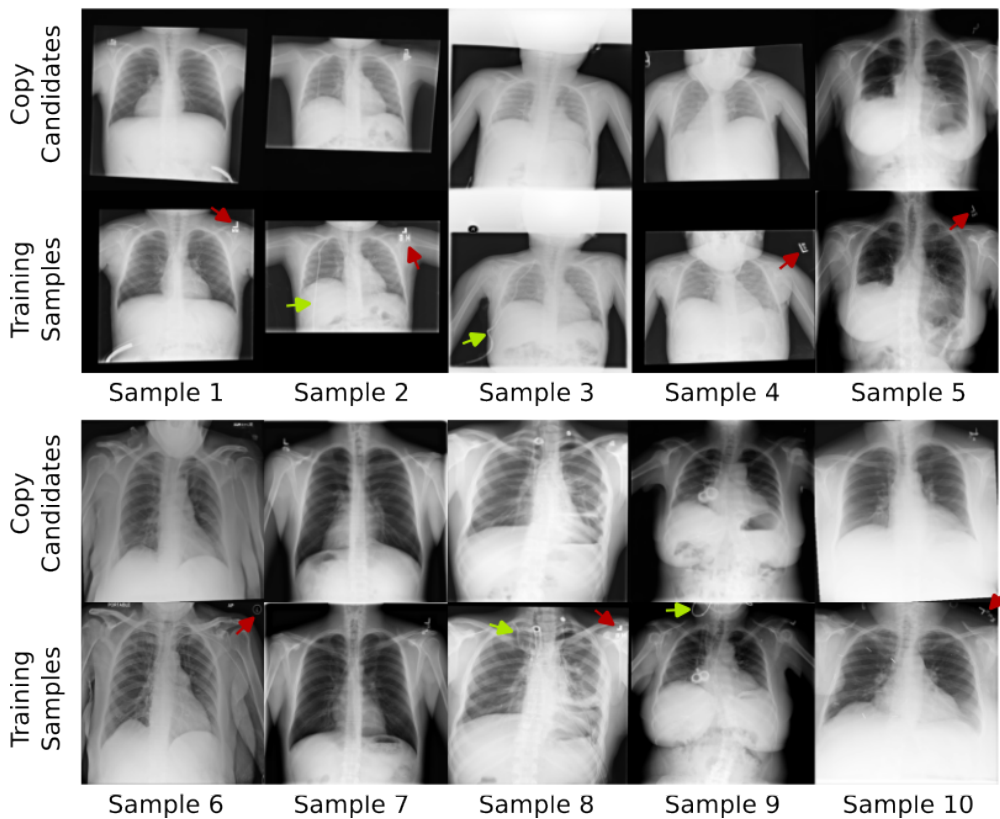


Figure 8: Representative cross sections of real and copy candidate samples in X-ray dataset. The augmented model generates copies that in addition to augmentations also produce minor variations (marked with arrows).

generalize well as they come across different variations of the training samples and this artificial expansion gives them the ability to generate samples that are not identical to the training samples but interpolations of different variations of the same sample. Another explanation could be related to the way such models are trained. LDMs are trained to perform denoising. In the case of augmentation, the model comes across variations of each training sample multiple times, and instead of finding a solution that produces denoised training images, the model can converge to a solution that is based on minimizing training error across all variations. This in turn can produce images that are not identical to a training sample or its variations, but rather a solution that is an average of all variations. This can potentially lead to the removal or blurriness of small structures. For instance, if we carefully observe samples 2, 3, 8, and 9 (Fig. 8 green markers), we can see that a structure that resembles a wire is present in the training samples but missing from the copies. Furthermore, in samples 1, 2, 4, 5, 6, 8, and 10 (Fig. 8 red markers), the alphabet 'L' at the top right corner is blurred out in the copies.

4 Discussion

In this work, we assessed memorization in unconditional latent diffusion models for medical image synthesis. Trained models were used to synthesize novel medical images, and potential copies were detected using self-supervised models based on contrastive learning approach. Our results obtained on different datasets covering various anatomies, resolutions, field of views, and modalities indicate that such models are prone to patient data memorization. Furthermore, our self-supervised models were able to identify copies among synthetic images with reasonable performance levels. Additional complementary analyses point out several factors that can have an impact on memorization. Increasing training dataset size and adding data augmentation operations reduced memorization, whereas over-training enhanced memorization. These results suggest that memorization could be mitigated to some extent with careful training.

Our results indicate that increasing training data size reduces memorization. On the surface, these findings seem to contradict Fernandez et al. [17]. However, a careful observation shows that there are several nuanced differences, which make the results incomparable. First, as opposed to the unconditional models used in our study, Fernandez et al. used conditional models. In Fernandez et al., text prompts were used from the training data, and multiple samples were synthesized per prompt. Then, identification ratio was defined for each sample as the ratio of the number of copies to the number of synthesized samples. This is very different from the way memorization is computed in our study, where samples are randomly synthesized and compared with all training samples to examine the percentage of training samples that are memorized and the percentage of synthesized samples that are copies. Therefore, given the nature of the models, we cannot directly compare our results with Fernandez et al. Another noteworthy observation is that from the figure provided by Fernandez et al. (Figure. 3), it is difficult to tell if the model trained on more samples has memorized more training samples. Nevertheless, our results align with the findings from the studies conducted in computer vision, where data scarcity was shown to have a positive correlation with data memorization [23].

Our results suggest some of the factors that affect memorization. Another avenue of research could be devising efficient privacy-preserving generative models. For privacy-preserved open-data sharing, Fernandez et al. [17] proposed a two-step approach. In the first step, a diffusion model was trained on real data and the synthesized samples were refined to contain only novel samples. These refined samples were then utilized to train a new model with the aim to synthesize completely novel data. While this approach reduces memorization, the quality of the samples synthesized by the second model trained on refined synthetic data can be compromised. One potential approach to mitigate memorization can be using differential private diffusion models [24, 25].

Patient data memorization in diffusion models can have broad implications. First, patients might not be comfortable making their data publicly available, which is one of the core reasons why generative models are deployed for open-data sharing in the first place. Incidentally sharing patient data copies defeats the whole purpose. Second, patient data copies among synthetic images can also be potentially traced back to the original patient leading to patient re-identification. Packhäuser et al. [9] were able to identify two X-ray images from the same patient acquired at different times even when the patient’s conditions altered. Using such approaches, an attacker can use partially available patient information to recover patient data copies among presumed novel synthetic data and recover sensitive clinical information.

Here, we primarily focused on memorization in unconditional diffusion models for medical image generation. Another future direction could be broadening our research to further include conditional diffusion models and compare memorization with unconditional diffusion models.

Acknowledgement: This work was supported through state funds approved by the State Parliament of Baden-Württemberg for the Innovation Campus Health + Life Science Alliance Heidelberg Mannheim, BMBF-SWAG Project 01KD2215D, and Informatics for life project through Klaus Tschira Foundation. The authors also gratefully acknowledge the data storage service SDS@hd supported by the Ministry of Science, Research and the Arts Baden-Württemberg (MWK) and the German Research Foundation (DFG) through grant INST 35/1314-1 FUGG and INST 35/1503-1 FUGG. The authors also acknowledge support by the state of Baden-Württemberg through bwHPC and the German Research Foundation (DFG) through grant INST 35/1597-1 FUGG.

References

- [1] J. Wolleb, R. Sandkühler, F. Bieder, P. Valmaggia, and P. C. Cattin, “Diffusion models for implicit image segmentation ensembles,” in *Proceedings of The 5th International Conference on Medical Imaging with Deep Learning*, ser. Proceedings of Machine Learning Research, E. Konukoglu, B. Menze, A. Venkataraman, C. Baumgartner, Q. Dou, and S. Albarqouni, Eds., vol. 172. PMLR, 06–08 Jul 2022, pp. 1336–1348.
- [2] A. Güngör, S. U. Dar, Şaban Öztürk, Y. Korkmaz, H. A. Bedel, G. Elmas, M. Ozbey, and T. Çukur, “Adaptive diffusion priors for accelerated mri reconstruction,” *Medical Image Analysis*, p. 102872, 2023.

- [3] M. Özbey, O. Dalmaz, S. U. Dar, H. A. Bedel, c. Öztürk, A. Güngör, and T. Çukur, “Unsupervised medical image translation with adversarial diffusion models,” *IEEE Transactions on Medical Imaging*, pp. 1–1, 2023.
- [4] J. Wolleb, F. Bieder, R. Sandkühler, and P. C. Cattin, “Diffusion models for medical anomaly detection,” in *Medical Image Computing and Computer Assisted Intervention – MICCAI 2022*, L. Wang, Q. Dou, P. T. Fletcher, S. Speidel, and S. Li, Eds. Cham: Springer Nature Switzerland, 2022, pp. 35–45.
- [5] A. Kazerouni, E. K. Aghdam, M. Heidari, R. Azad, M. Fayyaz, I. Hacihaliloglu, and D. Merhof, “Diffusion models in medical imaging: A comprehensive survey,” *Medical Image Analysis*, vol. 88, p. 102846, 2023.
- [6] W. H. L. Pinaya, P.-D. Tudosiu, J. Dafflon, P. F. Da Costa, V. Fernandez, P. Nachev, S. Ourselin, and M. J. Cardoso, “Brain Imaging Generation with Latent Diffusion Models,” in *Deep Generative Models*. Cham: Springer Nature Switzerland, 2022, pp. 117–126.
- [7] I. E. Hamamci, S. Er, E. Simsar, A. Tezcan, A. G. Simsek, F. Almas, S. N. Esirgun, H. Reynaud, S. Pati, C. Bluethgen *et al.*, “Generatect: Text-guided 3d chest ct generation,” *arXiv preprint arXiv:2305.16037*, 2023.
- [8] P. Chambon, C. Bluethgen, J.-B. Delbrouck, R. Van der Sluijs, M. Połacin, J. M. Z. Chaves, T. M. Abraham, S. Purohit, C. P. Langlotz, and A. Chaudhari, “Roentgen: Vision-language foundation model for chest x-ray generation,” 2022. [Online]. Available: <https://arxiv.org/abs/2211.12737>
- [9] K. Packhäuser, S. Gundel, N. Münster, C. Syben, V. Christlein, and A. Maier, “Deep learning-based patient re-identification is able to exploit the biometric nature of medical chest x-ray data,” *Scientific Reports*, vol. 12, no. 1, p. 14851, 2022.
- [10] A. Borji, “Pros and cons of gan evaluation measures: New developments,” *Computer Vision and Image Understanding*, vol. 215, p. 103329, 2022. [Online]. Available: <https://www.sciencedirect.com/science/article/pii/S1077314221001685>
- [11] N. Carlini, C. Liu, Ú. Erlingsson, J. Kos, and D. Song, “The secret sharer: Evaluating and testing unintended memorization in neural networks,” in *28th USENIX Security Symposium (USENIX Security 19)*. Santa Clara, CA: USENIX Association, Aug. 2019, pp. 267–284. [Online]. Available: <https://www.usenix.org/conference/usenixsecurity19/presentation/carlini>
- [12] S. U. H. Dar, A. Ghanaat, J. Kahmann, I. Ayx, T. Papavassiliou, S. O. Schoenberg, and S. Engelhardt, “Investigating data memorization in 3d latent diffusion models for medical image synthesis,” *arXiv preprint arXiv:2307.01148*, 2023.
- [13] S. U. H. Dar, I. Ayx, M. Kapusta, T. Papavassiliou, S. O. Schoenberg, and S. Engelhardt, “Effect of training epoch number on patient data memorization in unconditional latent diffusion models,” in *Bildverarbeitung für die Medizin 2024*, 2024.
- [14] M. U. Akbar, W. Wang, and A. Eklund, “Beware of diffusion models for synthesizing medical images—a comparison with gans in terms of memorizing brain tumor images,” *arXiv preprint arXiv:2305.07644*, 2023.
- [15] R. Rombach, A. Blattmann, D. Lorenz, P. Esser, and B. Ommer, “High-Resolution Image Synthesis with Latent Diffusion Models,” in *2022 IEEE/CVF Conference on Computer Vision and Pattern Recognition (CVPR)*, 2022, pp. 10 674–10 685.
- [16] J. Ho, A. Jain, and P. Abbeel, “Denoising Diffusion Probabilistic Models,” in *Advances in Neural Information Processing Systems*, H. Larochelle, M. Ranzato, R. Hadsell, M. F. Balcan, and H. Lin, Eds., vol. 33. Curran Associates, Inc., 2020, pp. 6840–6851.
- [17] V. Fernandez, P. Sanchez, W. H. L. Pinaya, G. Jacenków, S. A. Tsiftaris, and J. Cardoso, “Privacy distillation: Reducing re-identification risk of multimodal diffusion models,” *arXiv preprint arXiv:2306.01322*, 2023.
- [18] T. Chen, S. Kornblith, M. Norouzi, and G. Hinton, “A simple framework for contrastive learning of visual representations,” in *Proceedings of the 37th International Conference on Machine Learning*, ser. Proceedings of Machine Learning Research, H. D. III and A. Singh, Eds., vol. 119. PMLR, 13–18 Jul 2020, pp. 1597–1607. [Online]. Available: <https://proceedings.mlr.press/v119/chen20j.html>
- [19] X. Wang, Y. Peng, L. Lu, Z. Lu, M. Bagheri, and R. M. Summers, “Chestx-ray8: Hospital-scale chest x-ray database and benchmarks on weakly-supervised classification and localization of common thorax diseases,” in *Proceedings of the IEEE Conference on Computer Vision and Pattern Recognition (CVPR)*, July 2017.
- [20] N. Bien, P. Rajpurkar, R. L. Ball, J. Irvin, A. Park, E. Jones, M. Bereket, B. N. Patel, K. W. Yeom, K. Shpanskaya, S. Halabi, E. Zucker, G. Fanton, D. F. Amanatullah, C. F. Beaulieu, G. M. Riley, R. J. Stewart, F. G. Blankenberg, D. B. Larson, R. H. Jones, C. P. Langlotz, A. Y. Ng, and M. P. Lungren, “Deep-learning-assisted diagnosis for knee magnetic resonance imaging: Development and retrospective validation of mrnet,” *PLOS Medicine*, vol. 15, no. 11, pp. 1–19, 11 2018.

-
- [21] W. H. Pinaya, M. S. Graham, E. Kerfoot, P.-D. Tudosiu, J. Dafflon, V. Fernandez, P. Sanchez, J. Wolleb, P. F. da Costa, A. Patel *et al.*, “Generative ai for medical imaging: extending the monai framework,” *arXiv preprint arXiv:2307.15208*, 2023.
 - [22] F. Khader, G. Müller-Franzes, S. Tayebi Arasteh, T. Han, C. Haarbuerger, M. Schulze-Hagen, P. Schad, S. Engelhardt, B. Baeßler, S. Foersch, J. Stegmaier, C. Kuhl, S. Nebelung, J. N. Kather, and D. Truhn, “Denoising diffusion probabilistic models for 3D medical image generation,” *Scientific Reports*, vol. 13, no. 1, p. 7303, 2023.
 - [23] G. Somepalli, V. Singla, M. Goldblum, J. Geiping, and T. Goldstein, “Diffusion art or digital forgery? investigating data replication in diffusion models,” in *Proceedings of the IEEE/CVF Conference on Computer Vision and Pattern Recognition (CVPR)*, June 2023, pp. 6048–6058.
 - [24] T. Dockhorn, T. Cao, A. Vahdat, and K. Kreis, “Differentially Private Diffusion Models,” *Transactions on Machine Learning Research*, 2023. [Online]. Available: <https://openreview.net/forum?id=ZPpQk7FJXF>
 - [25] M. Tölle, U. Köthe, F. André, B. Meder, and S. Engelhardt, “Content-aware differential privacy with conditional invertible neural networks,” in *Distributed, Collaborative, and Federated Learning, and Affordable AI and Healthcare for Resource Diverse Global Health*. Cham: Springer Nature Switzerland, 2022, pp. 89–99.